Strain promoted azide alkyne cycloaddition, an efficient surface functionalization strategy for microRNA magnetic separation

Djamila Kechkeche, Sirine El Mousli, Claire Poujouly, Emilie Secret, Vincent Dupuis, Isabelle Le Potier, Marie-Emmanuelle Goriot, Julien Siracusa, Sébastien Banzet, Jean Gamby, et al.

Next Materials 6 (2025) 100409

Contents lists available at ScienceDirect

Next Materials

journal homepage: www.sciencedirect.com/journal/next-materials

Research article

Strain promoted azide alkyne cycloaddition, an efficient surface functionalization strategy for microRNA magnetic separation

Djamila Kechkeche [a,b], Sirine El Mousli [a], Claire Poujouly [b], Emilie Secret [a], Vincent Dupuis [a], Isabelle Le Potier [b], Marie-Emmanuelle Goriot [c,d], Julien Siracusa [c], Sébastien Banzet [c,d], Jean Gamby [b], Jean-Michel Siaugue [a,*]

[a] Sorbonne Université, CNRS, PHysico-chimie des Électrolytes et Nanosystèmes InterfaciauX (PHENIX), Paris F-75005, France
[b] Université Paris-Saclay, CNRS, Centre de Nanosciences et de Nanotechnologies (C2N), Palaiseau F-91120, France
[c] Institut de Recherche Biomédicale des Armées, Clamart F-92140, France
[d] UMR-MD-1197, INSERM, Université Paris Saclay, Ministère des armées, Clamart F-9214, France

ARTICLE INFO

Keywords:
Magnetic nanoparticles
Strain-promoted azide alkyne cycloaddition
SPAAC click chemistry
MicroRNA
Magnetic separation

ABSTRACT

In an emergency context, the detection of microRNA (miRNA), which are potential biomarkers of cardiovascular and muscular pathologies is hampered by the time required for the various steps involved: treatment of the patient sample, reverse transcription (RT), and finally polymerase chain reaction (PCR). In this context, magnetically assisted extraction of miRNA could shorten the sample treatment duration and enable a potential pre-concentration to gain in sensitivity. To this goal, magnetic nanoparticles (MNP) functionalized with DNA were developed. Maghemite nanoparticles were coated with a layer of silica, doubly functionalized with PEG chains to guarantee colloidal stability and limit non-specific protein adsorption, and amine functions to allow post-functionalization with DNA which have complementary sequences of the targeted miRNA. Two post-functionalization strategies were tested, one based on the reaction between a thiolated DNA and a maleimide group at the surface of the MNP, the other between an azide-functionalized DNA and a dibenzocyclooctyne group on the surface of the MNP. The strain-promoted azide alkyne cycloaddition (SPAAC click chemistry) proved to be the most efficient functionalization strategy. Optimization of the complementary DNA grafting protocol, carried out by varying the ratios between the quantities of dibenzocyclooctyne groups and DNA and between the quantities of DNA and MNP, revealed on the one hand that the quantity of DNA grafted per nanoparticle could be finely controlled, and on the other hand that the grafting on the MNP's surface of an excessive quantity of dibenzocyclooctyne groups led to a reduction in grafting yields. The optimized process was used for grafting the complementary DNA of 6 different miRNA, including 4 biomarkers of muscle injury (miR-1, 133a, 133b, and 206). It led to the grafting of approximately 4 complementary DNA per MNP, whatever the nucleotide sequence considered. Capture of the targeted miRNA by magnetic separation was then studied in buffered model media and in complex biological media. This study showed that MNP allowed magnetically-assisted extraction of target miRNA with good hybridization yields, even in biological media for which the capture capacity was preserved at around 75 %, with rapid kinetics and satisfactory selectivity.

1. Introduction

Recent studies have shown that microRNA (miRNA), which are nucleic acids of around twenty nucleotides involved in the control of gene expression, are potential biomarkers of numerous pathologies, including cancer, but also acute cardiovascular and muscular damage [1–4]. Their detection in emergency diagnostics is therefore considered, to confirm the diagnosis of extremely severe pathologies such as cardiovascular events. In the case of muscular pathologies, miRNA have been shown to be reliable indicators of muscle injury linked to intense exercise, and their diagnosis could prove invaluable in the very specific context of armed forces operations. It would be a decisive aid to decision-making before deploying substantial resources to evacuate wounded soldiers. The objective is to provide a rapid yet reliable method

* Corresponding author.
E-mail address: jean-michel.siaugue@sorbonne-universite.fr (J.-M. Siaugue).

https://doi.org/10.1016/j.nxmate.2024.100409
Received 13 May 2024; Received in revised form 2 October 2024; Accepted 22 October 2024
Available online 7 November 2024

for detecting highly specific miRNA, which can be implemented in isolated conditions, with limited resources in a critical situation.

The various emergency applications are currently not feasible because the standard technique for quantifying miRNA, *i.e.* reverse transcriptase quantitative polymerase chain reaction (RT-qPCR) [5], takes too long to complete (several hours). Additionally, it is a sophisticated technique that only highly qualified staff can use because it calls for expensive consumables and specific equipment. There is therefore a real interest in developing new, faster techniques for quantifying miRNA, and alternatives such as digital PCR (dPCR) or ultra-fast PCR are being studied [6,7]. However, these techniques are still dependent on the two steps prior to PCR: extraction of miRNA from the biological sample and reverse transcription of miRNA into complementary DNA.

The circulating miRNA that can be detected in blood are both numerous, due to their diversity, and present at extremely low concentrations. This explains why numerous PCR cycles are needed to quantify them, in a relative way, by measuring the concentrations of a number of miRNA against those of reference miRNA. An anomalous increase in the concentration of a miRNA compared with reference miRNA is thus indicative of a pathology [8]. This is a challenge in terms of the sensitivity and selectivity of the technique used. Treatment of the biological sample could prove crucial in this context, firstly by targeted extraction of specific miRNA from the biological medium, and secondly by pre-concentrating the extracted miRNA if they can be separated from the other components of the biological sample.

Magnetically-assisted extraction, also known as magnetic separation [9,10], is relevant from both these points of view, provided that a solid, magnetic and affine (*i.e.* selective) support is available for the species whose concentration is to be determined. The use of nanoparticles (NP) is particularly advantageous from this point of view because of their small size. This gives them an extremely high surface-to-volume ratio, *i.e.* a very large specific surface area, onto which the affine ligands for the species to be extracted can be grafted, in our case the complementary DNA sequences of the targeted miRNA. For an equivalent mass of solid support, this small size means that the smaller their size, the greater their extraction capacity, since the surface/volume ratio in the case of spherical NP is inversely proportional to their diameter. In addition, again because of its small size, this is a solid support, but one that diffuses by Brownian motion, leading to much faster capture kinetics than in the case of a conventional solid support, such as the surface of a well on a microtiter plate conventionally used in biological analysis. Our group has shown for example that the use of magnetic nanoparticles (MNP) with antigens grafted onto their surface leads to a 30-fold improved limit of detection of the targeted antibody, with the analysis being carried out in a few minutes compared to several hours for a conventional ELISA test [11]. To guarantee these gains in sensitivity and time, the stability of the colloidal dispersion must be maintained, even in complex biological environments.

Numerous applications of MNP in *in vitro* diagnostics have thus been reported, in which nanoparticles are used to preconcentrate the targeted entity or also to amplify the signal in certain electrochemical or optical-based immunoassays [12]. Moreover, they are already used clinically for *in vivo* diagnosis in MRI imaging, as T2 contrast agents, due to their intrinsic magnetic properties, and are being studied for multimodal imaging applications, combining MRI and PET imaging, for example [13]. A large number of magnetic nanometric platforms for targeted drug delivery have also been described in the literature, the most recent combining therapy and *in vivo* imaging, for applications in a field now referred to as theranostics [14]. Both the colloidal stabilization and the post-functionalization of MNP by ligands of biological interest, for example to carry out active targeting as a complement to passive targeting in targeted therapy [15], or to capture a target entity to be pre-concentrated, in *in vitro* diagnostics, require extremely precise control of the functionalization of the MNP surface.

Several approaches have been developed over the last few decades to achieve complex functionalization of the MNP surface [16]. One of the oldest approach is to functionalize the MNP with molecules or polymers of relatively low molecular weight that bears on one side chemical functions with high complexation constants for Fe(III) ions, enabling a strong affinity for the iron oxide surface, and on the other side reaction groups allowing subsequent post-functionalization [17]. An original example is the functionalization of maghemite NP with dimercaptosuccinic acid (DMSA), which has two carboxylic acid functions that can bind to iron (III) atoms on the surface, and which contributes to the colloidal stability of nanoparticles at physiological pH, which is essential for medical applications, by adding negative charges [18]. Interestingly, this molecule also has two thiol functions, enabling post-functionalization with a fluorophore, for example, to combine magnetic and fluorescence properties [19]. These two thiol functions also help to stabilize the functionalization by forming intermolecular disulfide bridges. Indeed, this approach suffers mainly from the lability of surface-anchored ligands, which can be displaced, particularly in a biological environment, leading to a loss of functionalization. The use of polydentate molecules or polymers with several chelating functions, such as carboxylic acid, catechol, or phosphonic acid functions, enables this desorption to be limited to a certain extent.

Another approach is to encapsulate magnetic nanoparticles and cover their surface with an organic or inorganic coating, thus resulting in composite nanoparticles. Biopolymers, like chitosan and dextran, have been widely used as organic coatings [20]. Chemical transformations of some of their functions, such as the oxidation of certain alcohols to aldehyde, allow their surface to be post-functionalized. Numerous polymers, both natural and synthetic, with specific properties, such as thermo-sensitivity for use in magnetic hyperthermia for targeted drug delivery, are also being widely studied [21].

Coating with a layer of silica to obtain MNP, sometimes referred to as core-shell MNP, is the most widespread example of covering the surface with an inorganic coating [22,23]. The silica layer is synthesized by hydrolysis and condensation of tetraethylorthosilicate (TEOS), usually at a basic pH, either in an alcoholic medium (Stöber process) [24,25] or in a water-in-oil microemulsion [26]. The silica layer synthesized in this way can be fluorescent by doping it with a fluorophore previously coupled to an organosilane, such as aminopropyltriethoxysilane (APTS). It can also have a controlled porosity by adding a structuring agent, such as cetyltrimethylammonium bromide (CTAB), during the synthesis of the silica layer [27]. This possibility has led to some very exciting developments in drug delivery, notably the development of mesoporous core-shell MNP, loaded with drugs, and whose pores are sealed using molecular gatekeepers [28]. The drugs could then be delivered on demand using magnetic hyperthermia, with local heating of the MNP causing the gates to open [29].

Furthermore, there is a large number of commercial organosilanes containing 3 ethoxy functions, involved in the hydrolysis and condensation processes, and another functionality, thus opening the way to the on-demand functionalization of the silica layer and therefore of the MNP surface. These include organosilanes containing polyethylene glycol chains or zwitterionic molecules, two types of functionalities that considerably increase the colloidal stability of nanoparticles and also their stealth in a biological environment by limiting the non-specific adsorption of proteins [30–32]. There are also similar compounds, but with a reacting group allowing subsequent coupling with other chemical entities, like biological ones (proteins, antibodies, DNA, etc.). The introduction of amine groups paves the way to carbodiimide chemistry and reactions with N-hydroxysuccinimide active esters [33] while those of thiol groups allows thiol-ene click chemistry [34] and reactions with maleimide derivatives. This latter method has been the subject of an in-depth study to optimize the grafting of peptides and antibodies onto the surface of polymeric NP, demonstrating its potential for functionalizing NP [35]. Finally, bio-orthogonal couplings are also accessible, the most often used being that between an alkyne and an azide. Usually, an additional surface functionalization step is carried out, for example by reacting amine functions with succinimide derivatives containing

alkyne or azide functions, as many compounds of this type are now commercially available. Although the reaction is sometimes carried out in the presence of a copper catalyst [36], according to the method initially developed by Sharpless *et al.* [37], the most common reaction is the strain-promoted azide alkyne cycloaddition (SPAAC click chemistry) proposed by Bertozzi *et al.* [38], [39]. This method consists of taking advantage of the greater reactivity of a constrained triple bond, thus eliminating the need for copper catalysis. There are many examples of MNP functionalized by SPAAC click chemistry for biomedical applications such as in *in vivo* diagnostics, in MRI [40] and PET [41], and in stem cell tracking and imaging [42,43], but less for *in vitro* diagnostics and in particular for surface functionalization by nucleotide sequences. SPAAC click chemistry has already been successfully used to graft MNP to the surface of DNA origami at selected positions [44]. In another study, it was demonstrated that this coupling strategy enabled single strands of DNA to be attached to the surface of magnetic nanoparticles by adjusting the grafting density [45].

In this work, we describe the synthesis of maghemite nanoparticles coated with a non-porous silica layer, the surface of which is doubly functionalized by short PEG chains on one hand, and by amine functions on the other. Our objective being the selective magnetic extraction of miRNA, the amine functions were used to graft complementary DNA strands of the targeted miRNA onto the surface. Alternative DNA capture strategies were not included in this study, although they have demonstrated their effectiveness for capturing oligonucleotides in biological environments. Notably, the use of magnetic nanoparticles functionalized with carboxylic acid groups [46,47] was not considered because, although it allows for efficient DNA capture, this capture is not selective and therefore does not enable targeting specific oligonucleotide sequences. Another approach involves functionalizing the surface of magnetic nanoparticles with streptavidin to capture biotinylated DNA sequences [48]. Since we aimed to use nanoparticles with the smallest possible hydrodynamic diameter to ensure the fastest possible capture kinetics, we did not consider this approach of grafting a relatively large protein onto the surface of the magnetic nanoparticles.

Two protocols were tested, one involving coupling between a maleimide group and a thiolated DNA, the other between a dibenzocyclooctyne group and an azide-functionalized DNA. As the latter protocol proved to be the most effective, it was studied in greater detail in order to optimize it and then used on several DNA, targeting miRNA biomarkers of muscle or cancer pathologies. In view of the urgent nature of muscle injury management, the miRNA considered were mainly muscle injury biomarkers (miR-1, 133a, 133b, 206), but a cardiac injury biomarker (miR-208a) and a liver injury biomarker (miR-122) were also included in the study in order to broaden its scope. Finally, the ability of the functionalized MNP to capture target DNA was assessed, both in a buffered environment and in a complex biological environment, as well as the kinetics and selectivity of capture.

2. Experimental section

2.1. Materials and methods

37 % hydrochloric acid, 52 % nitric acid, 22.5 % and 30 % ammonia, absolute ethanol, acetone, diethyl ether, anhydrous dimethylsulfoxyde (DMSO), iron(II) chloride, iron(III) nitrate nonahydrate, 27 % iron(III) chloride aqueous solution, sodium chloride, were purchased from VWR chemicals (Radnor, USA). 3-N-morpholinopropanesulfonic acid sodium salt (MOPS), N-2-hydroxyethylpiperazine-N-2-ethane sulfonic acid (HEPES), sodium citrate, tetraethoxyorthosilicate (TEOS), 3-aminopropyltriethoxysilane (APTS), fluorescamine, sulfosuccinimidyl-4-(N-maleimidomethyl)cyclohexane-1-carboxylate (Sulfo-SMCC), dibenzocyclooctyne-PEG$_4$-N-hydroxysuccinimidyl ester (DBCO) were purchased from Sigma Aldrich (Darmstadt, Germany). 90 % 3-[methoxy(polyethylenoxy)]propyltrimethoxysilane (PEOS) was purchased from ABCR (Karlsruhe, Germany).

MS Miltenyi columns were purchased from Myltenyi (Bergisch Gladbach, Germany). 30 kDa-cut-off-membrane filters were purchased from Sartorius (Goettingen, Germany).

Probe DNA with complementary sequences of targeted miRNA were purchased either from Eurogentec (Seraing, Belgium) for the 5' thiol-modified ones or from Integrated DNA Technologies (Coralville, USA) for the 5' azide-modified ones. The amount of probe DNA grafted on NP was determined using probe DNA labeled with fluorescein on the 3' end. A calibration curve was obtained by measuring the fluorescence intensity at 495 nm of several solutions with known probe DNA concentrations.

Target DNA mimicking the sequences of targeted miRNA were purchased from Eurogentec (Seraing, Belgium). The amount of target DNA hybridized on NP was determined using target DNA labeled with cyanine-5.5 (Cy5.5) on the 5' end. A calibration curve was obtained by measuring the fluorescence intensity at 645 nm of several solutions with known target DNA concentrations.

Due to the high cost of fluorescein and cyanine labeled DNA, the amount of grafted probe DNA and the amount of hybridized target DNA were measured only once by fluorescence for each condition studied. The reported values are therefore not derived from multiple experiments, and consequently, statistical analysis and significance cannot be performed.

All DNA samples were purchased in a dried format and diluted in deionized water to obtain a stock solution at a concentration of 10^{-4} M, stored in the freezer at −20°C.

Table 1 presents all the DNA sequences used in this work.

The morphology of the synthesized NP was characterized by transmission electron microscopy (TEM, JEOL 1011). A droplet of NP dispersion was deposited on a carbon-coated copper grid and air-dried at room temperature. Diameters were measured using ImageJ software ($n \geq 200$) and the data obtained were analyzed as the mean ± standard deviation (log normal law).

The total iron concentrations of all samples were measured by atomic absorption spectroscopy (AAS, PinAAcle 500, Perkin Elmer).

The magnetic properties of NP dispersed in water were measured using a Quantum Design Superconducting Quantum Interference Device (SQUID, MPMS-XL).

Dynamic light scattering (DLS) and zeta-potential measurements were performed on a Malvern Zetasizer instrument.

Fluorescence spectroscopy was performed on a SpectraMax i3x microplate reader from Molecular Devices.

The concentration of NP in each sample was calculated using the iron concentration of the stock solution of NP.

The concentration of amino functions in each sample was determined using fluorescamine assay [49]. A calibration curve was obtained by measuring the fluorescence intensity at 480 nm of several solutions with known APTS concentrations.

Table 1
Sequences of the probe and target DNA.

Name	Probe DNA sequences (5' to 3')	Target DNA sequences (5' to 3')
miR−122	CA AA CAC CAT TGT CAC ACT GC	GC AGT GTG ACA ATG GTG TT TG
miR−1	AT ACA TAC TTC TTT ACA TTC CA	TG GAA TGT AAA GAA GTA TGT AT
miR−133a	CA GCT GGT TGA AGG GGA CCA AA	TT TGG TCC CCT TCA ACC AGC TG
miR−133b	TA GCT GGT TGA AGG GGA CCA AA	TT TGG TCC CCT TCA ACC AGC TA
miR−206	CC ACA CAC TTC CTT ACA TTC CA	TG GAA TGT AAG GAA GTG TGT GG
miR−208a	AC AAG CTT TTT GCT CGT CTT AT	AT AAG ACG AGC AAA AAG CTT GT

2.2. Synthesis of maghemite NP

The size sorted maghemite NP were obtained by alkaline co-precipitation [50]. 22.5 % ammonia solution (1 L) was added to an acidic iron (II) and iron (III) ions solution (180 g of $FeCl_2$, 100 mL of 37 % hydrochloric acid, 500 mL of water and 715 mL of 27 % $FeCl_3$) and left at room temperature under stirring for 30 min. After rinsing with water, the obtained magnetite NP (Fe_3O_4) were redispersed in 360 mL of 52 % nitric acid, the solution was agitated for 10 min, and the NP were magnetically separated from the solution. Then a solution of $Fe(NO_3)_3$ (323 g) in water (800 mL) was added, and the combined mixture was boiled for 30 min to give maghemite NP (γ-Fe_2O_3).

The resulting NP were acidified with 52 % nitric acid (360 mL) and washed three times with acetone (3×1 L) and two times with diethyl ether (2×500 mL) before being redispersed in water (1 L), resulting in maghemite NP, which are polydispersed in size. To decrease the polydispersity, a size sorting process [51] was performed thanks to the addition of 52 % nitric acid (30 mL) to precipitate the larger particles. These precipitated NP were separated from the rest of the magnetic fluid, washed with acetone (3×500 mL) and diethyl ether (2×300 mL), and finally redispersed in water (125 mL). To ensure their stability and dispersion at neutral pH, the NP were citrated [52] by boiling the dispersion with sodium citrate (4.5 g) for 30 min. After washing with acetone (3×500 mL) and diethyl ether (2×300 mL), the resulting NP were dispersed in water (125 mL).

2.3. Synthesis of silica coated maghemite NP

Silica coated maghemite NP were synthesized using a procedure developed and optimized by our group [53,54]. 364 µL of size-sorted citrated maghemite NP ([Fe] = 1.9 M) were diluted in 30 mL of water and 60 mL of ethanol. 464 µL (2.05 mmol) of TEOS and 1.5 mL of 30 % ammonia were then added, and the mixture was left to react under vigorous stirring using an orbital shaker for two hours. Then, 185 µL (0.34 mmol) of PEOS, 81 µL of APTS (0.34 mmol), and 153 µL (0.68 mmol) of TEOS were added to the solution and left to react overnight. The obtained NP were washed three times with an ethanol/diethyl ether solution (1/15) and redispersed in 3 mL of MOPS buffer (pH = 7.3, [MOPS] = 100 mM).

2.4. Grafting of probe DNA

10 µL of the stock solution of silica coated maghemite NP ([Fe] = 0.123 mol/L) and the appropriate amount of a stock solution in anhydrous DMSO of sulfo-SMCC or DBCO were added to 100 µL of HEPES buffer (pH = 7.3, [HEPES] = 50 mM, [NaCl] = 500 mM). The solution was mixed for one hour at room temperature using an orbital shaker. Afterward, NP were recovered by ultrafiltration (13 000 rpm, 10 min) with a 30 kDa-cut-off membrane filter and redispersed in 100 µL of HEPES buffer.

The appropriate amount of the stock solution of probe DNA (0.3 µL or 0.6 µL according to the ratio DNA/NP) was added to 20 µL of this dispersion of NP in HEPES buffer. The solution was mixed overnight at room temperature using an orbital shaker. NP were then washed three times with HEPES buffer using MS Miltenyi columns to perform magnetic separation. NP were finally eluted with 200 µL of HEPES buffer, and fluorescence intensity was measured at 495 nm.

2.5. Capture of target DNA

The NP-probe DNA were hybridized in 200 µL of HEPES buffer with the same quantity of target DNA (0.3 µL or 0.6 µL of the stock solution of target DNA according to the ratio DNA/NP) as the quantity of probe DNA used in the grafting step. The solution was mixed for 30 minutes at room temperature using an orbital shaker. NP were then washed three times with HEPES buffer using MS Miltenyi columns to perform magnetic separation. NP were finally redispersed in 200 µL of HEPES buffer, and fluorescence intensity was measured at 645 nm.

3. Results and discussion

3.1. Synthesis of silica coated maghemite NP

The synthesis of silica-coated maghemite NP was achieved using a method developed by our group (Fig. 1) [53,54]. Maghemite NP are synthesized by co-precipitation of iron(II) and iron(III) chloride salts with ammonia [50] and then size sorted to obtain a narrower size distribution [51]. The obtained maghemite NP, with an average physical diameter of 12.6 nm (Fig. 2a), are then functionalized with sodium citrate [52] to obtain a dispersion of maghemite NP stable in aqueous phase at neutral pH.

The protocol for coating these NP with silica involves two steps. The silica layer is synthesized in the first step by hydrolysis and condensation of TEOS in an alcoholic medium in the presence of ammonia (Stöber process [24,25]). A silanized fluorophore, obtained for example by reaction between a fluorophore containing an isothiocyanate function and APTS, can be used in this step to obtain a fluorescent silica layer. It is thus possible to combine magnetic and fluorescence properties, which is particularly useful for cell internalization studies [55]. We have also shown that controlled aggregation of maghemite NP, by adding a salt to the synthesis medium in order to screen the electrostatic repulsive interactions, allows the shape of these core-shell NP to be modified [56].

Functionalization of the surface of this silica layer is achieved in the second step by simultaneous condensation of three organosilanes: PEOS to introduce PEG chains to improve the colloidal stability in a biological medium, APTS to introduce amine functions for post-functionalization, and finally TEOS to improve the cross-linking rate, so that this functionalization is not too labile, particularly by hydrolysis. In particular, we have shown that varying the ratio of PEOS and APTS concentrations can be used to finely tune the quantity of amine functions on the surface and consequently the zeta potential at neutral pH, as these are protonated and therefore a source of positive charges, counterbalancing the negative charges of the deprotonated silanol groups at this same pH [57].

Here, the silica coating was carried out without the addition of salts, resulting in roughly spherical silica coated NP with an average of two maghemite NP in their core and an average physical diameter of 26.5 nm (Fig. 2b). Characterization by dynamic light scattering revealed a hydrodynamic diameter of 43 nm, close to the average physical diameter, proving that the NP are not aggregated. A zeta potential of +18 mV was measured, corresponding to the protonation of the amine functions at neutral pH. The dispersion is stable over several months in a buffered medium (pH = 7.4) (Figure S1).

The iron concentration of the final dispersion is 0.123 mol/L, a quite high concentration for composite NP. The concentration of silica coated maghemite NP is calculated thanks to Eq. (1).

$$[NP] = ([Fe].M)/(2.\rho.N.v)) \quad (1)$$

with [Fe] the iron concentration of the final dispersion, M the molar mass of maghemite (160 g/mol), r the volumic mass of maghemite (5.1×10^3 g/L), N the mean number of maghemite NP in the core (2) and v, the volume of a maghemite nanoparticle (spherical, d=12.3 nm).

The calculated concentration is of 1.65×10^{-6} mol/L of NP. The concentration of amine functions in the final dispersion, determined by fluorescence measurements after reaction with fluorescamine [49], is of 4.06×10^{-3} mol/L. The ratio of these two concentrations indicates that each silica coated NP bears approximately 2500 amine functions on its surface, *i.e.* approximately 1.1 amine functions/nm^2.

The magnetic properties of the silica coated NP are similar to those of maghemite NP, with a saturation magnetization of 59 emu/g(Fe_2O_3), zero remanent magnetization and zero coercive field, as expected for

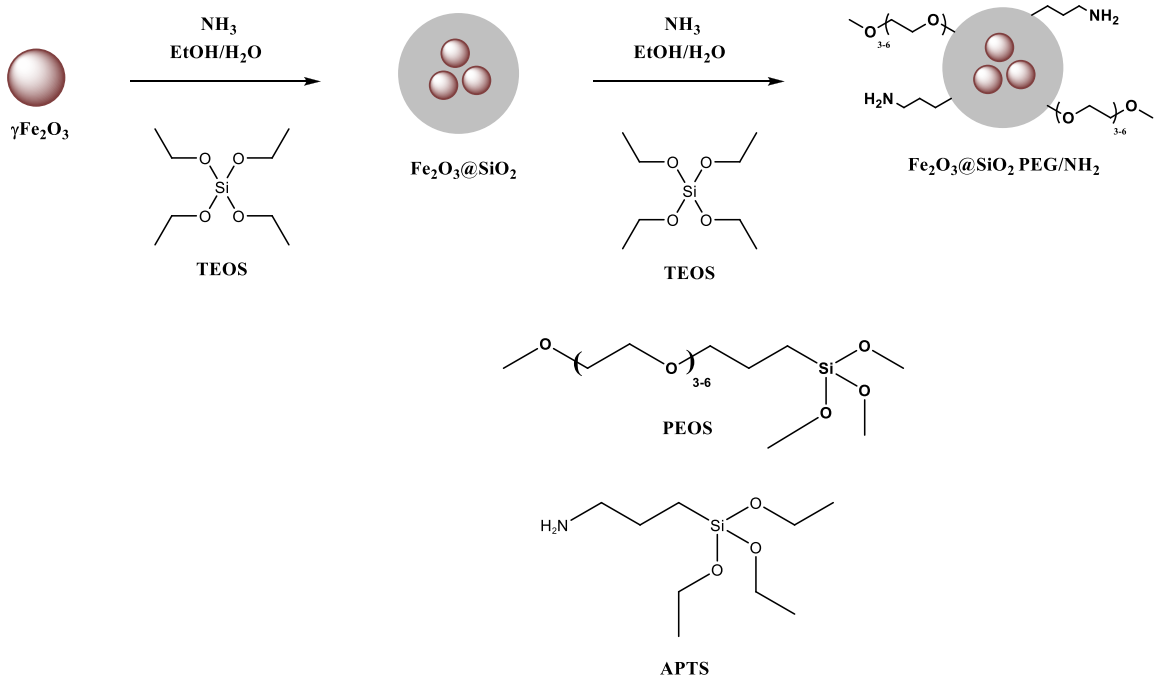

Fig. 1. Two-step synthesis procedure of silica coated maghemite NP.

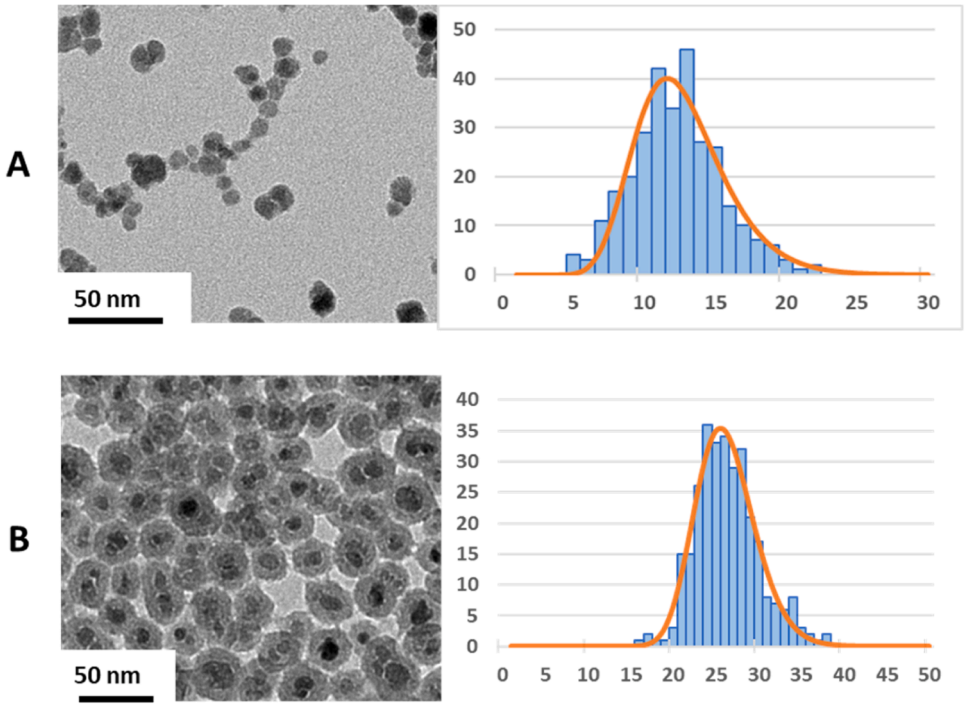

Fig. 2. TEM micrograph and size distribution of maghemite NP (A) and silica coated maghemite NP (B).

maghemite NP of this size, which are superparamagnetic at room temperature (Figure S1) [58].

3.2. Grafting of probe DNA

Probe DNA were grafted using two different strategies, one employing an amine/thiol heterolinker and the other an amine/azide heterolinker. The use of an amine/amine homolinker, such as glutaldehyde, to graft a probe DNA containing an amine function at the 5′ end onto the surface of the NP was not tried. Indeed, the use of such a homolinker could have resulted in coupling reactions between NP, leading to the formation of irreversible aggregates, made up of nanoparticles linked together by covalent bonds.

The first grafting strategy (Fig. 3) tested consisted of the reaction in a first step between the amine functions of the NP and sulfo-SMCC. This heterolinker has an N-hydroxysuccinimide group, reactive towards the amine functions of the NP, and a maleimide group, reactive towards the thiol functions of the DNA. This step is achieved in buffer by simply

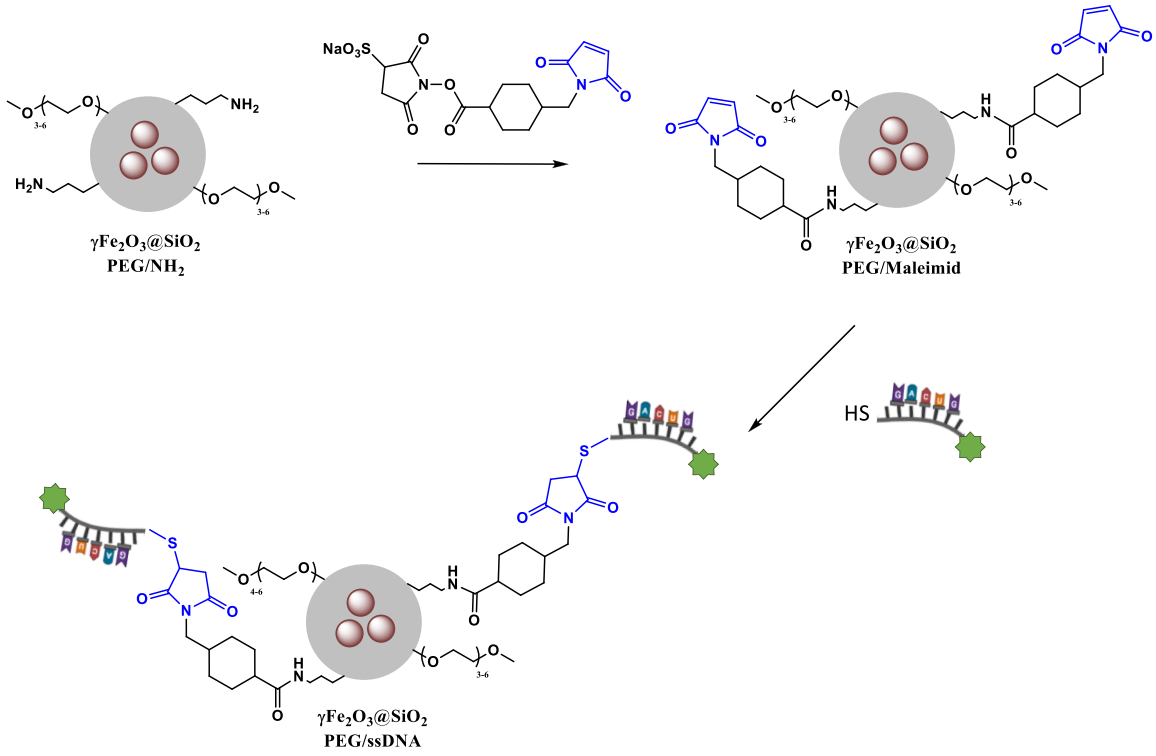

Fig. 3. Grafting of probe DNA using sulfo-SMCC and thiol modified probe DNA.

mixing the solution of NP and the appropriate quantity of a stock solution of sulfo-SMCC in anhydrous DMSO, at room temperature, for 1 hour. The NP are then purified by ultrafiltration to remove any excess of unreacted sulfo-SMCC.

The second step involves the reaction between the maleimide groups, now present on the surface of the NP, and probe DNA, modified at the 5′ end by a thiol function, and bearing a fluorophore, fluorescein, at the 3′ end. This step is achieved in buffer by adding an appropriate quantity of a stock solution of probe DNA in water to the NP dispersion. The mixture is stirred overnight at room temperature, and then the NP are purified by magnetic separation to eliminate ungrafted probe DNA.

For each sample of NP functionalized like this, the quantity of grafted DNA can be deduced from the calibration curve by measuring the fluorescence intensity. Knowing the quantity of NP introduced, calculated using Eq. (1), it is possible to calculate the quantity of grafted probe DNA/NP, neglecting any losses of NP during the purification stages by ultrafiltration at the first stage and by magnetic separation at the second stage. Different ratios between the quantities of sulfo-SMCC and probe DNA, for a constant ratio between the quantity of probe DNA and NP, equal to 9, were tested and the results obtained are reported in Fig. 4A.

Increasing the ratio of sulfo-SMCC to probe DNA did not improve the amount of probe DNA grafted to the surface of the NP, which stayed at around 1–1.5 grafted probe DNA/NP corresponding to a low grafting yield of around 10–15 %. It is not possible to control the amount of grafted probe DNA/NP by adjusting the ratio between the amounts of sulfo-SMCC and probe DNA. This disappointing result may be due to partial hydrolysis of the maleimide groups, leading to ring opening and formation of a maleic acid amide derivative that is not reactive towards thiol groups [59–61]. This has already been reported, particularly for certain alkaline pH values above 8, but also during the purification of liposomes containing maleimide functions on the surface [62]. The observed reduction in the reactivity of maleimide groups can therefore be due to their partial hydrolysis, maybe during purification by ultrafiltration in the first step.

An alternative grafting strategy (Fig. 5) was therefore tested using DBCO, an heterolinker containing, like sulfo-SMCC, an N-hydroxysuccinimide moiety that is reactive towards the amine functions of the NP, but which other moiety is a dibenzocyclooctyne group. This group enables cycloaddition with molecules containing an azide function,

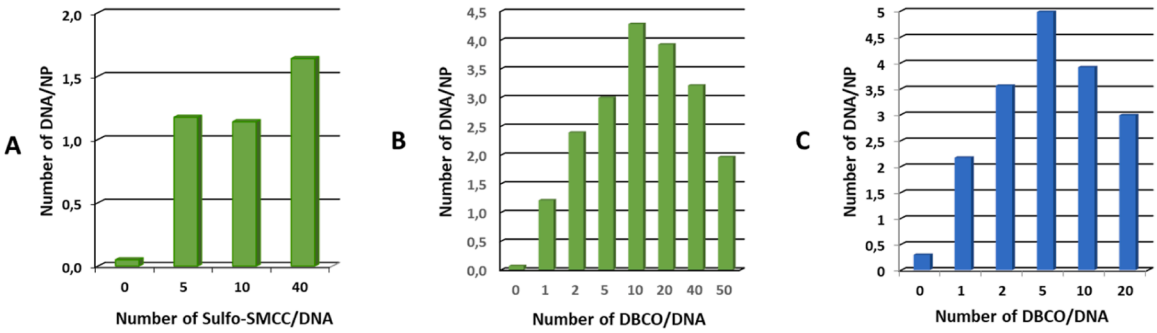

Fig. 4. Number of probe DNA grafted per NP according to the ratio between sulfo-SMCC and probe DNA quantities (A) or DBCO and probe DNA quantities (B, C) with 9 (A, B) or 18 (C) probe DNA per NP. These results were obtained for the grafting of the probe DNA for miR-122.

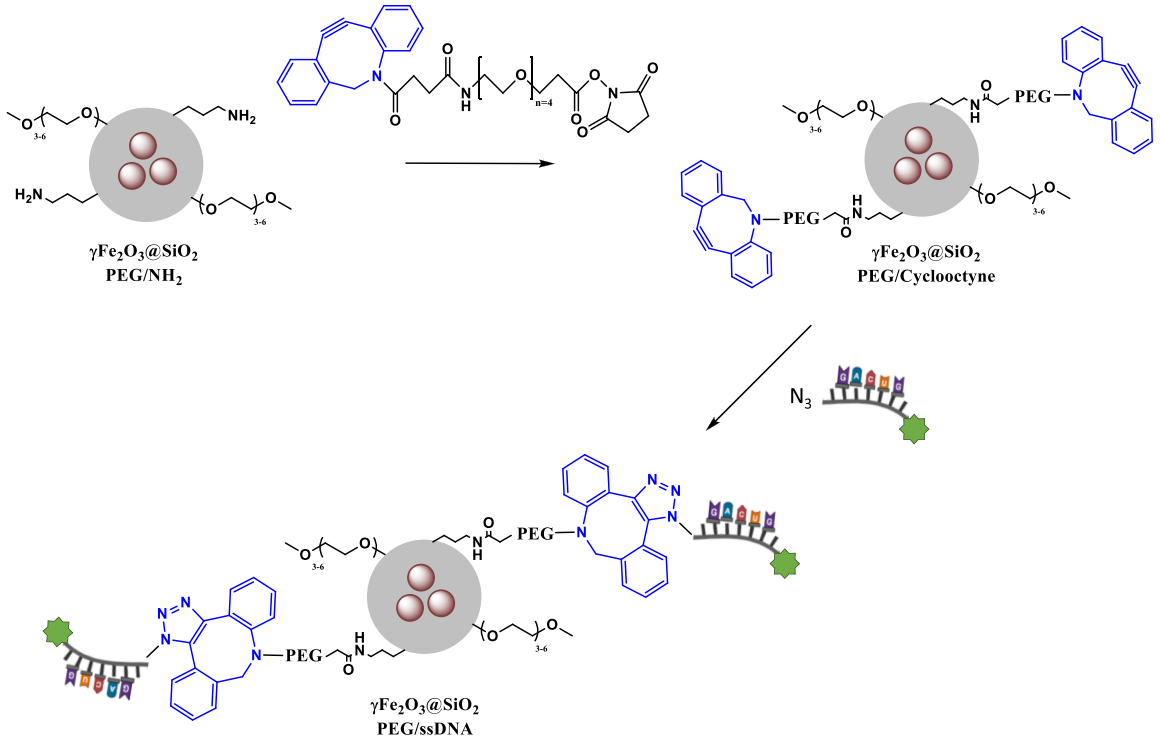

Fig. 5. Grafting of probe DNA using DBCO and azide modified probe DNA.

without copper catalysis, thanks to the enhanced reactivity of the constrained triple bond [38,39]. The two grafting steps were carried out in a similar way, substituting DBCO for sulfo-SMCC, and probe DNA of the same sequence, but modified at the 5′ end by an azide function, instead of a thiol function.

As before, these probe DNA contained fluorescein at the 3′ end in order to be able to quantify the probe DNA grafted in this way. The quantities of grafted DNA/NP were calculated by neglecting any losses of NP during the purification stages by ultrafiltration in the first stage and by magnetic separation in the second stage. Different DBCO/probe DNA ratios for a constant probe DNA/NP quantity equal to 9 were tested, and the results obtained are shown in Fig. 4B.

Increasing the ratio between the quantities of DBCO and probe DNA improved the grafting yield, which reached a maximum of around 48 % at a ratio of 10, corresponding to around 4 probe DNA grafted/NP. Interestingly, this grafting yield and therefore the quantity of probe DNA grafted decrease above this ratio of 10 DBCO/probe DNA, first modestly and then much more drastically at 50 DBCO/probe DNA. At this value, partial precipitation of the NP is observed, indicating NP aggregation. A progressive aggregation of the NP at a ratio greater than 10 could explain the decrease in grafting yield, due to the decrease in the ratio/surface volume and the quantity of DBCO accessible for probe DNA grafting. This aggregation may be due to the very hydrophobic nature of the dibenzocyclooctyne group, which destabilizes the NP in aqueous media.

In order to optimize the amount of grafted probe DNA/NP, the same grafting protocol was tested for twice the amount of probe DNA/NP, *i.e.* 18, by similarly adjusting the amount of DBCO to the amount of probe DNA used. The results obtained are shown in Fig. 4C. The same phenomenon is observed, *i.e.* a rapid increase in grafting yield, followed by a decrease beyond the limit value of the DBCO/probe DNA ratio, equal to 5.

The same detailed study was also carried out for a different probe DNA, with a sequence complementary to that of miR-133a, in order to ensure that these results were not dependent on the oligonucleotide sequence studied. The influence of the DBCO/probe DNA quantities ratio on the amount of probe DNA grafted was therefore studied for miR-133a under the two conditions previously tested for miR-122, *i.e.* 9 probe DNA/NP and 18 probe DNA/NP. The results are shown in Figure S2. The quantities of probe DNA grafted are fairly close to those obtained for miR-122. Once again, the maximum grafting yield was obtained for the same two ratios between the quantities of DBCO and probe DNA, *i.e.* 10 for 9 probe DNA/NP and 5 for 18 probe DNA/NP.

So, for these two probe DNA, miR-122 and miR-133a, which have been the subject of a detailed study, the maximum amount of grafted DNA achieved using 18 DNA/NP is approximately equal to 5 DNA/NP. However, using double the amount of DNA/NP, although it leads to a slight increase in the number of grafted DNA, results in a decrease in grafting efficiency.

In order to compare the results of these two grafting protocols, involving 9 and 18 probe DNA/NP respectively, the results obtained were expressed as a function of the ratio between the quantities of DBCO and NP, for the 4 values common to the two protocols, for the two values of the ratio between the quantities of probe DNA and NP, and for the two miRNA tested. The grafting yields were calculated by comparing the amount of grafted probe DNA to the amount of introduced probe DNA for each tested condition. They are expressed as a percentage and are indicated in parentheses (Table 2).

Table 2
Number of probe DNA grafted per NP and grafting yields for miR-122 and miR-133a.

	miR-122		miR-133	
DBCO/NP	**9 DNA/NP**	**18 DNA/NP**	**9 DNA/NP**	**18 DNA/NP**
18	2.39 (26.6 %)	2.17 (12.1 %)	2.08 (23.1 %)	2.14 (11.9 %)
90	4.28 (47.6 %)	4.98 (27.7 %)	3.90 (43.3 %)	5.41 (30.1 %)
180	3.92 (43.6 %)	3.91 (21.7 %)	2.20 (24.4 %)	4.72 (26.2 %)
360	3.21 (35.7 %)	2.99 (16.6 %)	1.26 (14.0 %)	2.7 (15.0 %)

This comparison shows that maximum grafting yield is achieved for the same limiting value of this ratio, equal to 90. Destabilization of the NP, or even reduced accessibility of the DBCO groups on the surface, when the ratio between the quantities of DBCO and NP is too high, are therefore responsible for the reduction in the quantity of grafted probe DNA. The fact that similar quantities of probe DNA are grafted for a ratio between the quantities of DBCO and probe DNA equal to 5 or 10 (90 DBCO/NP), but also equal to 1 or 2 (18 DBCO/NP) indicates that the reactivity of the azide functions with respect to the DBCO functions, in any case under the conditions tested in this work, is satisfactory and is not responsible for the reduction in grafting yields above the limit value of 90 DBCO/NP.

Although the optimum quantity of grafted probe DNA, equal to approximately 5, was obtained for 18 probe DNA/NP and 5 DBCO/probe DNA (DBCO/NP = 90), these were not the conditions finally chosen because of the lower grafting yield and the high cost of custom oligonucleotide sequences. The conditions selected, 10 DBCO/probe DNA and 9 DNA/NP (DBCO/NP = 90), which allow the grafting of 4.28 probe DNA/NP and 3.90 probe DNA/NP for miR-122 and 133a, with grafting yields of 47.6 % and 43.3 %, respectively, were used for the grafting of the 4 other DNA sequences studied, complementary to miR-1, 133b, 206, and 208a (Table 3).

The grafting yields of the 6 probe DNA with sequences complementary to the targeted miRNA were between 42.4 % and 54.0 %, corresponding to quantities of grafted probe DNA of between 3.82 and 4.86 probe DNA/NP. This corresponds, when calculating the average across all these probe DNA grafting experiments, without considering the diversity of sequences, which are nevertheless of similar lengths, to an average grafted probe DNA value of 4.22 and a standard deviation of 0.34. In view of the diversity of nucleotide sequences, it can be concluded that this grafting method can be generalized to any nucleotide sequences, provided that it contains an azide function at its 3′ or 5′ end.

3.3. Capture of target DNA

All the nanoparticles considered during optimization of the grafting protocol by SPAAC click chemistry, therefore containing probe DNA on the surface complementary to miR-122 or 133a, were tested for capture by hybridization. Target DNA mimicking the sequences of the targeted miRNA were used because of their better stability. The NPs were first functionalized using the conditions described in the previous section, but with probe DNA that did not contain fluorescein at the 3′ end. The quantities of target DNA captured by hybridization were measured by fluorescence, using nucleotides sequences containing a 5.5 cyanine at the 5′ end. The use of NP containing fluorescent probe DNA was therefore avoided, in order to ensure that the fluorescence intensity measured corresponded to the capture of target DNA.

Hybridization with nucleotide sequences was carried out in buffer at room temperature under agitation for 30 minutes. A preliminary experiment revealed rapid capture kinetics, with the quantity of target DNA hybridized to the surface of the nanoparticles reaching a plateau after 15 minutes of reaction (Figure S3). This rapid kinetic was expected for colloidal objects diffusing in solution due to their Brownian motion. Our group has already reported a much faster capture kinetic of the corresponding antibodies for antigen-functionalized NP, compared to a capture at the surface of a non-diffusing solid support [11]. The quantities of target DNA captured, for the two grafting protocols at 9 and 18 probe DNA/NP are shown in Fig. 6, for miR-122, and in figure S4, for miR-133a. They are shown superimposed on the quantities of probe DNA grafted during the previous step, as a function of the DBCO/probe DNA ratio, so that the efficiency of the hybridization process on the surface of the NP can be assessed visually.

The amount of target DNA hybridized increases approximately in the same way as the amount of probe DNA grafted to the surface of the NP in the first step, indicating that the hybridization yield is approximately constant whatever the amount of probe DNA grafted to the surface of the NP. This means that the surface-grafted probe DNA are accessible and correctly oriented for hybridization with the target DNA.

The use of a higher quantity of probe DNA, equal to 18 probe DNA/NP, during the probe DNA grafting step does not allow a significant increase in the quantity of target DNA captured. As the quantities of probe DNA grafted are approximately the same as for 9 probe DNA/NP, this means that for the NP obtained for these two grafting protocols, the hybridization yield of the probe DNA with the target DNA is similar.

Similar hybridization results were obtained for the second miRNA studied in more detail, miR-133a, and the results obtained are shown in Figure S4. As before, it is possible to compare the results obtained for these two grafting protocols and for these two miRNA, by expressing the results obtained as a function of the DBCO/NP ratio for the 4 values common to both protocols. The hybridization yields were calculated by comparing the amount of target DNA captured to the amount of grafted probe DNA. They are expressed as a percentage and are indicated in parentheses (Table 4). A comparison of all these results shows that the quantities of target DNA captured are highest for the DBCO/NP ratio value equal to 90, which is logical since this corresponds to NP containing the most probe DNA on the surface. On the other hand, it is also interesting to note that hybridization yields barely change, always remaining approximately between 50 % and 65 %, with the exception of the values measured for the DBCO/NP ratio equal to 18, for which the quantities of target DNA hybridized are sometimes lower, particularly for miR-133a.

Table 5 shows the quantities of target DNA hybridized for the 6 different miRNA studied, with only the optimized grafting conditions (10 DBCO/probe DNA and 9 DNA/NP) used for the other DNA sequences studied, complementary to miR-1, 133b, 206 and 208a.

Observation of both the quantities of target DNA captured and the hybridization yields shows that this method of grafting probe DNA and then capturing target DNA gives satisfactory and similar results for all 6 different miRNA studied, with around two to three target DNA hybridized/NP and hybridization yields of between 49.5 % and 62.9 %.

This quantity of target DNA captured by nanoparticles can also be expressed in terms of the surface area occupied by each DNA double strand. Given that a NP has a surface area of around 2000 nm^2, the occupation of this surface area by a few DNA double strands corresponds for each of them to an occupied surface area of several hundred nm^2, a surface area that seems much greater than that corresponding to a DNA double strand, composed of around twenty bases, which can be estimated at a maximum of a few tens of nm^2. However, this reduced capture capacity has already been observed for surfaces functionalized by PEG chains whose flexibility limits adsorption, so that total coverage of the surface cannot be achieved [35]. In addition, the configuration adopted by the PEG chains (brush or mushroom) is dependent on their surface density and leads to the occupation of different surfaces on the NP [63–65]. Although PEG chains probably limit the extraction capacity of NP, they are nevertheless essential for stabilizing nanoparticles, particularly in a biological environment, and for limiting non-specific adsorption phenomena.

In order to explore the potential of this method, the study was extended by considering the influence of the medium in which capture takes place. In the case of biological samples, the miRNA will be

Table 3
Number of probe DNA grafted per NP and grafting yields for the six different miRNA studied.

		Probe DNA/NP	Grafting yield (%)
Liver	miR−122	4.28	47.6
Skeletal/cardiac muscle	miR−1	4.3	47.8
Skeletal/cardiac muscle	miR−133a	3.90	46.3
Skeletal muscle	miR−133b	4.86	54.0
Skeletal muscle	miR−206	4.18	46.4
Cardiac muscle	miR−208a	3.82	42.4

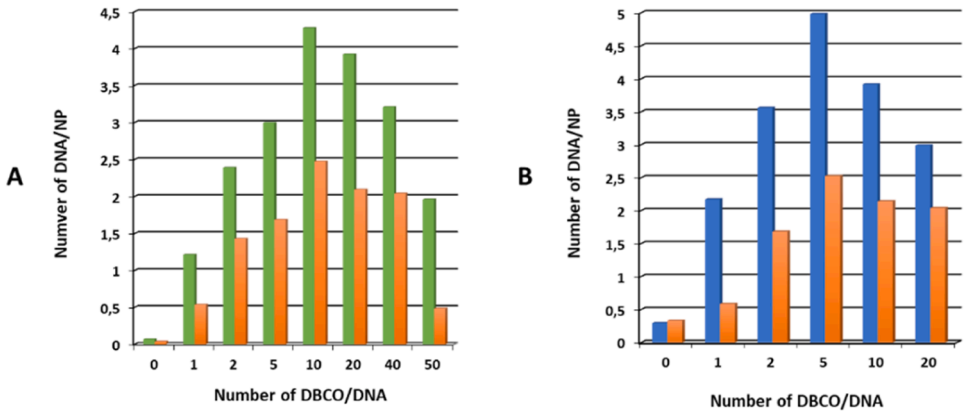

Fig. 6. Number of probe DNA grafted per NP (in green (A) or blue (B)) and target DNA captured per NP (in orange) according to the ratio between DBCO and probe DNA quantities with 9 (A) or 18 (B) DNA per NP. These results were obtained for miR-122.

Table 4
Number of target DNA captured per NP and hybridization yields for miR-122 and miR-133a.

	miR-122		miR-133	
DBCO/NP	**9 DNA/NP**	**18 DNA/NP**	**9 DNA/NP**	**18 DNA/NP**
18	1.43 (60.1 %)	0.59 (27.2 %)	0.83 (39.9 %)	0.69 (32.2 %)
90	2.47 (57.8 %)	2.52 (50.6 %)	1.93 (49.5 %)	3.43 (63.4 %)
180	2.09 (53.3 %)	2.14 (54.7 %)	1.04 (47.3 %)	2.61 (55.3 %)
360	2.04 (63.6 %)	2.04 (68.2 %)	0.69 (54.8 %)	1.61 (59.6 %)

Table 5
Number of target DNA captured per NP and hybridization yields for the six different miRNA studied.

		Target DNA/NP	Hybridization yield (%)
Liver	miR−122	2.47	57.8
Skeletal/cardiac muscle	miR−1	2.38	55.3
Skeletal/cardiac muscle	miR−133a	1.93	49.5
Skeletal muscle	miR−133b	2.78	57.2
Skeletal muscle	miR−206	2.63	62.9
Cardiac muscle	miR−208a	2.20	57.6

extracted not in a model medium, but in a complex medium containing proteins and antibodies that may adsorb non-specifically to the surface of the NP. We therefore tested the extraction of two of the miRNA studied in two complex media, bovine fetal serum and rat plasma. For miR-122, 1.81 and 1.96 target DNA/NP were extracted, *i.e.* 73 % and 79 % of the extraction capacity in buffer (2.47 target DNA/NP), in bovine fetal serum and rat plasma, respectively. Similar results were obtained for miR-208a, for which 1.65 and 1.68 target DNA/NP were extracted, in bovine fetal serum and rat plasma, respectively, compared to 2.20 target DNA/NP extracted in buffer, *i.e.* approximately 75 % of the extraction capacity in buffer. This excellent preservation of the extraction capacity in a biological environment containing many other species likely to interact non-specifically with the surface of the NP is attributable to the presence of PEG chains, a source of repulsive interactions, which contribute to the colloidal stability of the nanoparticles but also limit the non-specific adsorption phenomena. Our group has already obtained similar results in a study aimed at antibody capture by antigen-functionalized nanoparticles. In particular, we showed that by adjusting the APTS/PEOS ratio during the surface functionalization step, and thus modifying the surface density of the PEG chains, it was possible to significantly reduce the non-specific interactions of the surface with proteins [66].

The capture selectivity of probe DNA on the surface was also studied using NP functionalized by probe DNA under the conditions involving the most DNA during the functionalization step, *i.e.* 18 probe DNA/NP for a ratio between the quantities of DBCO and probe DNA equal to 5. Our idea was to obtain the maximum amount of probe DNA on the surface, despite the corresponding low grafting yield, in order to test their selectivity. The miR-133a target was chosen for this study in order to assess the capture selectivity of its complementary DNA with respect to miR-133b, which was also studied and differs from miR-133a by only one nucleotide. The capture capacity of these NP was evaluated against miR-133a, as a reference, and then against miR-122 and miR-133b in mismatch capture experiments. It was also determined in competition experiments involving mixtures of the target sequence, miR-133a, and the closest non-complementary sequence, mir 133b, in variable proportions (Table 6).

The results obtained show that miR-133a is selectively captured, but only to a certain extent. In fact, only miR-122, whose sequence is very different from miR-133a, is not captured at all by the NP. In the case of miR-133b, it is indeed captured, but with a lower hybridization rate of 39.4 % instead of 62.4 %. Competition experiments show that reducing the ratio between the quantities of miR-133a and miR-133b, from 2 (1/0.5) to 0.5 (1/2), results in a reduction in the hybridization yield of miR-133a from 55.9 % to 28.0 %, indicating that an increasing proportion of probe DNA is hybridized with the miR-133b sequence. To improve capture selectivity in this very unfavorable configuration, with a single nucleotide differentiating miR-133a from miR-133b, it would be possible to use modified complementary DNA, including locked nucleic acids (LNA) nucleotides, which bind more strongly to DNA than standard DNA and could therefore possess a higher affinity for the targeted miRNA [67].

Table 6
Number of DNA captured per NP and hybridization yields for mismatch and competition experiments.

		DNA/NP	Hybridization yield (%)
Reference	miR−133a	3.34	62.4
Mismatch	miR−122	0	0
	miR−133b	2.11	39.4
Competition	miR−133a/miR−133b 1/0.5	2.99	55.9
	miR−133a/miR−133b 1/1	1.93	36
	miR−133a/miR−133b 1/2	1.5	28

4. Conclusions

In this work, MNP were functionalized with DNA complementary to six different miRNA, most of which are biomarkers of muscular injury. To achieve this, size-sorted maghemite nanoparticles were coated with a layer of silica, the surface of which was doubly functionalized with amine functions and PEG chains. Two methods were studied for grafting the complementary DNA of two of the miRNA studied under varying experimental conditions, in terms of the ratio between the quantities of DNA and reagents, and also the ratio between the quantities of DNA and MNP. The first method studied involved the reaction between a thiol DNA and a maleimide group, while the second involved an azide DNA and a constrained triple bond. Strain-promoted azide alkyne cycloaddition, *i.e.* SPAAC click chemistry, proved to be the most successful method, enabling the grafting of around 4 DNA per nanoparticle with a yield of around 50 % for all the nucleotide sequences considered, thanks to the optimized experimental conditions. Moreover, optimization of the experimental conditions showed that the quantity of probe DNA grafted could be finely controlled and that the use of an excessive quantity of DBCO led to a reduction in grafting yields.

These probe DNA-functionalized MNP enabled the magnetically-assisted extraction of around 2 target DNA per nanoparticle, both in a buffered model environment and in a complex biological environment. The presence of PEG chains on the surface of MNP ensures colloidal stability and limits non-specific adsorption of proteins, thereby preserving extraction capacity and fast extraction kinetics in a biological environment.

These functionalized MNP could prove particularly useful as pre-concentration agents for certain miRNA in future bioassays combining magnetic separation and rapid quantification of miRNA for diagnosis in emergency situations.

CRediT authorship contribution statement

Djamila Kechkeche: Formal analysis, Investigation, Visualization. **Sirine El Mousli:** Formal analysis, Investigation. **Claire Poujouly**: Formal analysis, Investigation, Visualization. **Emilie Secret:** Conceptualization, Methodology, Validation, Writing: review & editing, Visualization, Supervision, Funding acquisition. **Vincent Dupuis:** Conceptualization, Methodology, Validation, Writing: review & editing, Visualization, Supervision, Funding acquisition. **Isabelle Le Potier:** Methodology, Validation. **Emmanuelle Goriot**: Investigation. **Julien Siracusa:** Methodology, Validation. **Sébastien Banzet:** Conceptualization, Methodology, Validation, Writing: review & editing, Supervision, Funding acquisition. **Jean Gamby:** Conceptualization, Methodology, Validation, Writing: review & editing, Visualization, Supervision, Funding acquisition, Project administration. **Jean-Michel Siaugue:** Conceptualization, Methodology, Validation, Writing: original draft, Writing: review & editing, Visualization, Supervision, Funding acquisition.

Declaration of Competing Interest

The authors declare that they have no known competing financial interests or personal relationships that could have appeared to influence the work reported in this paper.

Acknowledgements

We are thankful to David Hrabovsky at the MPBT (Physical Measurements at Low Temperatures) platform of Sorbonne Université for his assistance with magnetism measurements and to Aude Michel-Tourgis and Delphine Talbot for their help during total iron concentration measurements by AAS. This work is supported by a public grant overseen from the French National Research Agency (ANR) (DIMELEC project (ANR-19-CE09-0016)) and by the "Investissements d'Avenir" program (Labex NanoSaclay (ANR-10-LABX-0035)).

Appendix A. Supporting information

Supplementary data associated with this article can be found in the online version at doi:10.1016/j.nxmate.2024.100409.

References

[1] M. Li, J. Li, X. Ding, M. He, S.-Y. Cheng, microRNA and cancer, AAPS J. 12 (2010) 309–317, https://doi.org/10.1208/s12248-010-9194-0.
[2] Y. Yang, T. Yu, S. Jiang, Y. Zhang, M. Li, N. Tang, M. Ponnusamy, J.-X. Wang, P.-F. Li, miRNAs as potential therapeutic targets and diagnostic biomarkers for cardiovascular disease with a particular focus on WO2010091204, Expert Opin. Ther. Pat. 27 (2017) 1021–1029, https://doi.org/10.1080/13543776.2017.1344217.
[3] J. Siracusa, N. Koulmann, S. Banzet, Circulating myomiRs: a new class of biomarkers to monitor skeletal muscle in physiology and medicine, J. Cachex Sarcopenia Muscle 9 (2018) 20–27, https://doi.org/10.1002/jcsm.12227.
[4] P.-K. Min, S.Y. Chan, The biology of circulating microRNAs in cardiovascular disease, Eur. J. Clin. Investig. 45 (2015) 860–874, https://doi.org/10.1111/eci.12475.
[5] M. Arya, I.S. Shergill, M. Williamson, L. Gommersall, N. Arya, H.R.H. Patel, Basic principles of real-time quantitative PCR, Expert Rev. Mol. Diagn. 5 (2005) 209–219, https://doi.org/10.1586/14737159.5.2.209.
[6] E. Day, P.H. Dear, F. McCaughan, Digital PCR strategies in the development and analysis of molecular biomarkers for personalized medicine, Methods 59 (2013) 101–107, https://doi.org/10.1016/j.ymeth.2012.08.001.
[7] H. Wu, S. Zhang, Y. Chen, C. Qian, Y. Liu, H. Shen, Z. Wang, J. Ping, J. Wu, Y. Zhang, H. Chen, Progress in molecular detection with high-speed nucleic acids thermocyclers, J. Pharm. Biomed. Anal. 190 (2020) 113489, https://doi.org/10.1016/j.jpba.2020.113489.
[8] L. Moldovan, K.E. Batte, J. Trgovcich, J. Wisler, C.B. Marsh, M. Piper, Methodological challenges in utilizing miRNAs as circulating biomarkers, J. Cell. Mol. Med. 18 (2014) 371–390, https://doi.org/10.1111/jcmm.12236.
[9] L. Borlido, A.M. Azevedo, A.C.A. Roque, M.R. Aires-Barros, Magnetic separations in biotechnology, Biotechnol. Adv. 31 (2013) 1374–1385, https://doi.org/10.1016/j.biotechadv.2013.05.009.
[10] Lei Wang, Jianhan Lin, Recent advances on magnetic nanobead based biosensors: From separation to detection, TrAC Trends Anal. Chem. 128 (2020) 115915, https://doi.org/10.1016/j.trac.2020.115915.
[11] B. Teste, F. Malloggi, J.-M. Siaugue, A. Varenne, F. Kanoufi, S. Descroix, Microchip integrating magnetic nanoparticles for allergy diagnosis, Lab Chip 11 (2011) 4207–4213, https://doi.org/10.1039/C1LC20809H.
[12] E.M. Materon, C.M. Miyazaki, O. Carr, N. Joshi, P.H.S. Picciani, C.J. Dalmaschio, F. Davis, F.M. Shimizu, Magnetic nanoparticles in biomedical applications: a review, Appl. Surf. Sci. Adv. 6 (2021) 100163, https://doi.org/10.1016/j.apsadv.2021.100163.
[13] T.-H. Shin, Y. Choi, S. Kim, J. Cheon, Recent advances in magnetic nanoparticle-based multi-modal imaging, Chem. Soc. Rev. 44 (2015) 4501–4516, https://doi.org/10.1039/C4CS00345D.
[14] V.F. Cardoso, A. Francesko, C. Ribeiro, M. Bañobre-López, P. Martins, S. Lanceros-Mendez, Advances in magnetic nanoparticles for biomedical applications, Adv. Healthc. Mater. 7 (2018) 1700845, https://doi.org/10.1002/adhm.201700845.
[15] A. Farzin, S.A. Etesami, J. Quint, A. Memic, A. Tamayol, Magnetic nanoparticles in cancer therapy and diagnosis, Adv. Healthc. Mater. 9 (2020) 1901058, https://doi.org/10.1002/adhm.201901058.
[16] S. Liu, B. Yu, S. Wang, Y. Shen, H. Cong, Preparation, surface functionalization and application of Fe_3O_4 magnetic nanoparticles, Adv. Colloid Interface Sci. 281 (2020) 10216, https://doi.org/10.1016/j.cis.2020.102165.
[17] S.P. Pujari, L. Scheres, A.T.M. Marcelis, H. Zuilhof, Covalent surface modification of oxide surfaces, Angew. Chem. Int. Ed. 53 (2014) 6322–6356, https://doi.org/10.1002/anie.201306709.
[18] N. Fauconnier, J.N. Pons, J. Roger, A. Bee, Thiolation of maghemite nanoparticles by dimercaptosuccinic acid, J. Colloid Interface Sci. 194 (1997) 427–433, https://doi.org/10.1006/jcis.1997.5125.
[19] F. Bertorelle, C. Wilhelm, J. Roger, F. Gazeau, C. Ménager, V. Cabuil, Fluorescence-modified superparamagnetic nanoparticles: intracellular uptake and use in cellular imaging, Langmuir 22 (2006) 5385–5391, https://doi.org/10.1021/la052710u.
[20] R.P. Gambhir, S.S. Rohiwal, A.P. Tiwari, Multifunctional surface functionalized magnetic iron oxide nanoparticles for biomedical applications: a review, Appl. Surf. Sci. Adv. 11 (2022) 100303, https://doi.org/10.1016/j.apsadv.2022.100303.
[21] B.T. Mai, S. Fernandes, P.B. Balakrishnan, T. Pellegrino, Nanosystems based on magnetic nanoparticles and thermo- or pH responsive polymers: an update and future perspectives, Account Chem. Res. 51 (2018) 999–1013, https://doi.org/10.1021/acs.accounts.7b00549.
[22] A. Guerrero-Martınez, J. Perez-Juste, L.M. Liz-Marzan, Recent progress on silica coating of nanoparticles and related nanomaterials, Adv. Mater. 22 (2010) 1182–1195, https://doi.org/10.1002/adma.200901263.
[23] B.K. Sodipo, A.A. Aziz, Recent advances in synthesis and surface modification of superparamagnetic iron oxide nanoparticles with silica, J. Magn. Magn. Mater. 416 (2016) 275–291, https://doi.org/10.1016/j.jmmm.2016.05.019.

[24] W. Stöber, A. Fink, E. Bohn, Controlled growth of monodisperse silica spheres in the micron size range, J. Colloid Interface Sci. 26 (1968) 62–69, https://doi.org/10.1016/0021-9797(68)90272-5.

[25] A.P. Philipse, M.P.B. van Bruggen, C. Pathmamanoharan, Magnetic silica dispersions: preparation and stability of surface-modified silica particles with a magnetic core, Langmuir 10 (1994) 92–99, https://doi.org/10.1021/la00013a014.

[26] H.L. Ding, Y.X. Zhang, S. Wang, J.M. Xu, S.C. Xu, G.H. Li, Fe_3O_4@SiO_2 core/shell nanoparticles: the silica coating regulations with a single core for different core sizes and shell thicknesses, Chem. Mater. 24 (2012) 4572–4580, https://doi.org/10.1021/cm302828d.

[27] R.K. Singh, K.D. Patel, K.W. Leong, H.-W. Kim, Progress in nanotheranostics based on mesoporous silica nanomaterial platforms, ACS Appl. Mater. Interfaces 9 (2017) 10309–10337, https://doi.org/10.1021/acsami.6b16505.

[28] A. García-Fernandez, E. Aznar, R. Martinez-Manez, F. Sancenon, New advances in in vivo applications of gated mesoporous silica as drug delivery nanocarriers, Small 16 (2020) 1902242, https://doi.org/10.1002/smll.201902242.

[29] C.R. Thomas, D.P. Ferris, J.-H. Lee, E. Choi, M.H. Cho, E.S. Kim, J.F. Stoddart, J.-S. Shin, J. Cheon, J.I. Zink, Noninvasive remote-controlled release of drug molecules in vitro using magnetic actuation of mechanized nanoparticles, J. Am. Chem. Soc. 132 (2010) 10623–10625, https://doi.org/10.1021/ja1022267.

[30] J. Mosayebi, M. Kiyasatfar, S. Laurent, Synthesis, functionalization, and design of magnetic nanoparticles for theranostic applications, Adv. Healthc. Mater. 6 (2017) 1700306, https://doi.org/10.1002/adhm.201700306.

[31] Q. Li, C. Wen, J. Yang, X. Zhou, Y. Zhu, J. Zheng, G. Cheng, J. Bai, T. Xu, J. Ji, S. Jiang, L. Zhang, P. Zhang, Zwitterionic biomaterials, Chem. Rev. 122 (2022) 17073–17154, https://doi.org/10.1021/acs.chemrev.2c00344.

[32] S. El Mousli, Y. Dorant, E. Bertuit, E. Secret, J.-M. Siaugue, Silica-coated magnetic nanorods with zwitterionic surface functionalization to overcome non-specific protein adsorption, J. Magn. Magn. Mater. 589 (2024) 171571, https://doi.org/10.1016/j.jmmm.2023.171571.

[33] N. Kohler, C. Sun, J. Wang, M. Zhang, Methotrexate-modified superparamagnetic NPs and their intracellular uptake into human cancer cells, Langmuir 21 (2005) 8858–8864, https://doi.org/10.1021/la0503451.

[34] R.D. Rutledge, C.L. Warner, J.W. Pittman, R.S. Addleman, M. Engelhard, W. Chouyyok, M.G. Warner, Thiol-Ene induced diphosphonic acid functionalization of superparamagnetic iron oxide nanoparticles, Langmuir 26 (2010) 12285–12292, https://doi.org/10.1021/la101362y.

[35] L. Martinez-Jothar, S. Doulkeridou, R.M. Schiffelers, J.S. Torano, S. Oliveira, C. F. van Nostrum, W.E. Hennink, Insights into maleimide-thiol conjugation chemistry: conditions for efficient surface functionalization of nanoparticles for receptor targeting, J. Control. Release 282 (2018) 101–109, https://doi.org/10.1016/j.jconrel.2018.03.002.

[36] J. Wei, X. Shuai, R. Wang, X. He, Y. Li, M. Ding, J. Li, H. Tan, Q. Fu, Clickable and imageable multiblock polymer micelles with magnetically guided and PEG-switched targeting and release property for precise tumor theranosis, Biomaterials 145 (2017) 138–153, https://doi.org/10.1016/j.biomaterials.2017.08.005.

[37] V.V. Rostovtsev, L.G. Green, V.V. Fokin, K.B. Sharpless, A stepwise huisgen cycloaddition process: copper(I)-catalyzed regioselective "ligation" of azides and terminal alkynes, Angew. Chem. Int. Ed. 41 (2002) 2596–2599, https://doi.org/10.1002/1521-3773(20020715)41:14%3C2596::AID-ANIE2596%3E3.0.CO;2-4.

[38] N.J. Agard, J.A. Prescher, C.R. Bertozzi, A strain promoted [3 + 2] azide-alkyne cycloaddition for covalent modification of biomolecules in living systems, J. Am. Chem. Soc. 126 (2004) 15046–15047, https://doi.org/10.1021/ja044996f.

[39] J. Idiago-Lopez, E. Moreno-Antolın, J.M. de la Fuente, R.M. Fratila, Nanoparticles and bioorthogonal chemistry joining forces for improved biomedical applications, Nanoscale Adv. 3 (2021) 1261–1292, https://doi.org/10.1039/d0na00873g.

[40] J. Gallo, N. Kamaly, I. Lavdas, E. Stevens, Q.De Nguyen, M. Wylezinska-Arridge, E. O. Aboagye, N.J. Long, CXCR4-targeted and MMP-responsive iron oxide nanoparticles for enhanced magnetic resonance imaging, Angew. Chem. Int. Ed. 53 (2014) 9550–9554, https://doi.org/10.1002/anie.201405442.

[41] S.B. Lee, H.L. Kim, H.J. Jeong, S.T. Lim, M.H. Sohn, D.W. Kim, Mesoporous silica nanoparticle pretargeting for PET imaging based on a rapid bioorthogonal reaction in a living body, Angew. Chem. Int. Ed. 52 (2013) 10549–10552, https://doi.org/10.1002/anie.201304026.

[42] S. Lee, H.I. Yoon, J.H. Na, S. Jeon, S. Lim, H. Koo, S.S. Han, S.W. Kang, S.J. Park, S. H. Moon, J.H. Park, Y.W. Cho, B.S. Kim, S.K. Kim, T. Lee, D. Kim, S. Lee, M. G. Pomper, I.C. Kwon, K. Kim, In vivo stem cell tracking with imageable nanoparticles that bind bioorthogonal chemical receptors on the stem cell surface, Biomaterials 139 (2017) 12–29, https://doi.org/10.1016/j.biomaterials.2017.05.050.

[43] S. Lim, H.Y. Yoon, H.J. Jang, S. Song, W. Kim, J. Park, K.E. Lee, S. Jeon, S. Lee, D.-K. Lim, B.-S. Kim, D.-E. Kim, K. Kim, Dual-modal imaging-guided precise tracking of bioorthogonally labeled mesenchymal stem cells in mouse brain stroke, ACS Nano 13 (2019) 10991–11007, https://doi.org/10.1021/acsnano.9b02173.

[44] T.A. Meyer, C. Zhang, G. Bao, Y. Ke, Programmable assembly of iron oxide nanoparticles using DNA origami, Nano Lett. 20 (2020) 2799–2805.

[45] A. Lak, Y. Wang, P.J. Kolbeck, C. Pauer, M.S. Chowdhury, M. Cassani, F. Ludwig, T. Viereck, F. Selbach, P. Tinnefeld, M. Schilling, T. Lied, J. Tavacolib, J. Lipfer, Cooperative dynamics of DNA-grafted magnetic nanoparticles optimize magnetic biosensing and coupling to DNA origami, Nanoscale (15) (2024) 7678–7689.

[46] T.R. Sarkar, J. Irudayaraj, Carboxyl-coated magnetic nanoparticles for mRNA isolation and extraction of supercoiled plasmid DNA, Anal. Biochem. 379 (2008) 130–132, https://doi.org/10.1016/j.ab.2008.04.016.

[47] Z. Zhou, a,b, U.S. Kadam, J. Irudayaraj, One-stop genomic DNA extraction by salicylic acid-coated magnetic nanoparticles, Anal. Biochem. 442 (2013) 249–252, https://doi.org/10.1016/j.ab.2013.07.030.

[48] P. Gong, Z. Peng, Y. Wang, R. Qiao, W. Mao, H. Qian, M. Zhang, C. Li, S. Shi, Synthesis of streptavidin-conjugated magnetic nanoparticles for DNA detection, J. Nanopart. Res. 15 (2013) 1558, https://doi.org/10.1007/s11051-013-1558-9.

[49] M. Le Jeune, E. Secret, M. Trichet, A. Michel, D. Ravault, F. Illien, J.-M. Siaugue, S. Sagan, F. Burlina, C. Ménager, Conjugation of Oligo-His peptides to magnetic γ-Fe_2O_3@SiO_2 core-shell nanoparticles promotes their access to the cytosol, ACS Appl. Mater. Interfaces 14 (2022) 15021–15034, https://doi.org/10.1021/acsami.2c01346.

[50] R. Massart, E. Dubois, V. Cabuil, E. Hasmonay, Preparation and properties of monodisperse magnetic fluids, J. Magn. Magn. Mater. 149 (1995) 1–5, https://doi.org/10.1016/0304-8853(95)00316-9.

[51] S. Lefebure, E. Dubois, V. Cabuil, S. Neveu, R. Massart, Monodisperse magnetic nanoparticles: Preparation and dispersion in water and oils, J. Mater. Res. 13 (1998) 2975–2981, https://doi.org/10.1557/JMR.1998.0407.

[52] N. Fauconnier, A. Bee, J. Roger, J.N. Pons, Adsorption of gluconic and citric acids on maghemite particles in aqueous medium. Adsorption of gluconic and citric acids on maghemite particles in aqueous medium, in: C. Solans, M.R. Infante, M. J. García-Celma (Eds.), Trends in Colloid and Interface Science X. Progress in Colloid & Polymer Science, 100, Steinkopff, 1996, pp. 212–216, https://doi.org/10.1007/BFb0115782.

[53] V. Maurice, T. Georgelin, J.-M. Siaugue, V. Cabuil, Synthesis and characterization of functionalized core–shell γFe_2O_3–SiO_2 nanoparticles, J. Magn. Magn. Mater. 321 (2009) 1408–1413, https://doi.org/10.1016/j.jmmm.2009.02.051.

[54] T. Georgelin, S. Bombard, J.-M. Siaugue, V. Cabuil, Nanoparticle-Mediated Delivery of Bleomycin, Angew. Chem. Int. Ed. 49 (2010) 8897–8901, https://doi.org/10.1002/anie.201003316.

[55] H. Schöneborn, F. Raudzus, E. Secret, N. Otten, A. Michel, J. Fresnais, C. Ménager, J.-M. Siaugue, H. Zaehres, I.D. Dietzel, R. Heumann, Novel Tools towards Magnetic Guidance of Neurite Growth: (I) Guidance of Magnetic Nanoparticles into Neurite Extensions of Induced Human Neurons and In Vitro Functionalization with RAS Regulating Proteins, J. Funct. Biomater. 10 (2019) 32, https://doi.org/10.3390/jfb10030032.

[56] M.-C. Horny, J. Gamby, V. Dupuis, J.-M. Siaugue, Magnetic Hyperthermia on γ-Fe_2O_3@SiO_2 Core-Shell Nanoparticles for mi-RNA 122 Detection, Nanomaterials 11 (2021) 149, https://doi.org/10.3390/nano11010149.

[57] F. d'Orlyé, A. Varenne, T. Georgelin, J.-M. Siaugue, B. Teste, S. Descroix, P. Gareil, Charge-based characterization of nanometric cationic bifunctional maghemite/silica core/shell particles by capillary zone electrophoresis 30 (2009) 2572–2582, https://doi.org/10.1002/elps.200800835.

[58] L. Wu, A. Mendoza-Garcia, Q. Li, S. Sun, Organic Phase Syntheses of Magnetic Nanoparticles and Their Applications, Chem. Rev. 116 (2016) 10473–10512, https://doi.org/10.1021/acs.chemrev.5b00687.

[59] C.P. Ryan, M.E. Smith, F.F. Schumacher, D. Grohmann, D. Papaioannou, G. Waksman, F. Werner, J.R. Baker, S. Caddick, Tunable reagents for multi-functional bioconjugation: reversible or permanent chemical modification of proteins and peptides by control of maleimide hydrolysis, Chem. Commun. 47 (2011) 5452–5454, https://doi.org/10.1039/C1CC11114K.

[60] O. Koniev, A. Wagner, Developments and recent advancements in the field of endogenous amino acid selective bond forming reactions for bioconjugation, Chem. Soc. Rev. 44 (2015) 5495–5551, https://doi.org/10.1039/C5CS00048C.

[61] S. Matsui, H. Aida, Hydrolysis of some N-alkylmaleimides, J. Chem. Soc. Perkin Trans. 2 (1978) 1277–1280, https://doi.org/10.1039/P29780001277.

[62] M. Oswald, S. Geissler, A. Goepferich, Determination of the activity of maleimide functionalized phospholipids during preparation of liposomes, Int. J. Pharm. 514 (2016) 93–102, https://doi.org/10.1016/j.ijpharm.2016.06.116.

[63] J.M. Rabanel, P. Hildgen, X. Banquy, Assessment of PEG on polymeric particles surface, a key step in drug carrier translation, J. Control. Release 185 (2014) 71–87, https://doi.org/10.1016/j.jconrel.2014.04.017.

[64] S. Stolnik, B. Daudali, A. Arien, J. Whetstone, C.R. Heald, M.C. Garnett, S.S. Davis, L. Illum, The effect of surface coverage and conformation of poly(ethylene oxide) (PEO) chains of poloxamer 407 on the biological fate of model colloidal drug carriers, Biochim. Biophys. Acta, 2001, 1514, 261-279. Biochim. Et. Biophys. Acta (BBA) - Biomembr. 1514 (2001) 261–279, https://doi.org/10.1016/S0005-2736(01)00376-5.

[65] J.L. Perry, K.G. Reuter, M.P. Kai, K.P. Herlihy, S.W. Jones, J.C. Luft, M. Napier, J. E. Bear, J.M. DeSimone, PEGylated PRINT nanoparticles: the impact of PEG density on protein binding, macrophage association, biodistribution, and pharmacokinetics, Nano Lett. 12 (2012) 5304–5310, https://doi.org/10.1021/nl302638g.

[66] B. Teste, F. Kanoufi, S. Descroix, P. Poncet, T. Georgelin, J.-M. Siaugue, J. Petr, A. Varenne, M.-C. Hennion, Kinetic analyses and performance of a colloidal magnetic nanoparticle based immunoassay dedicated to allergy diagnosis, Anal. Bioanal. Chem. 400 (2011) 3395–3407, https://doi.org/10.1007/s00216-011-5021-4.

[67] J. Prout, M. Tian, A. Palladino, J. Wright, J.F. Thompson, LNA blockers for improved amplification selectivity, Sci. Rep. 13 (2023) 4858, https://doi.org/10.1038/s41598-023-31871-7.